

1 **Visualisation of developmental ossification using trace element mapping**

2 Jennifer Anné*¹, Nicholas P. Edwards¹, Arjen van Veelen^{1,2}, Victoria M. Egerton^{1,3}, Phillip L.
3 Manning^{1,3}, J. Fredrick W. Mosselmans⁴, Stephen Parry⁴, William I. Sellers¹, Michael Buckley¹,
4 Roy A. Wogelius¹

5

6 ¹University of Manchester, School of Earth and Environmental Science, Interdisciplinary Centre
7 for Ancient Life, Manchester M13 9PL, UK

8 ²University of Southampton, Faculty of Engineering and the Environment, Southampton, SO17
9 1BJ, UK

10 ³Department of Geology and Environmental Geoscience, College of Charleston, 66 George St,
11 Charleston, SC 29424, USA

12 ⁴Diamond Light Source, Didcot, OX11 0DE, UK

13

14 * jennifer.anne@manchester.ac.uk

15

16 **1. Specimens**

17 Specimens consisted of frozen 1-day old mice (*Mus musculus*) purchased from the Monkifield



18 Nutrition distributor (animal feed company; fig. S1). The forelimb was removed and skinned to

19 expose the bone and cartilage using a sterile scalpel and a dissecting scope. They were then
20 freeze-dried to prevent rotting while scanning at the synchrotron.

21 Figure S1: 1-day old mouse used in experiment.

22

23 The fossil fish (*Knightia eoceana*) was collected from Fossil Lake basin of the 50 million year old
24 Green River Formation of Wyoming, USA (fig. S2). The sample was analysed as it was extracted
25 from the site with no further preparation, washing, or application of glues or preservatives. Both
26 specimens are housed at the University of Manchester.

27



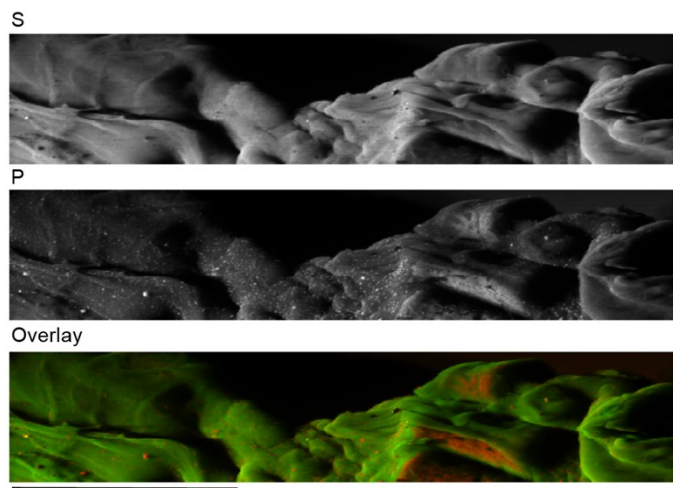
28

29 Figure S2: 50 million year old green river fish, *Knightia eoceana* (UM868).

30

31 2. Synchrotron XRF Low-Z maps *M. musculus*

32 P is distributed only within the ossified tissues of the phalanges and upper arm bones, though
33 such a distinction is difficult to see without overlaying P with another low-Z element (fig. S2).



34

35 Figure S3: Elemental maps of P and S in *M. musculus* distal radius and ulna and carpal bones.

36 Scan area is the same as in figure 1. S is evenly distributed throughout the soft tissues, while P is

37 concentrated mostly in the ossified tissues. This correlation can only be viewed in the overlay of

38 S (green) and P (red). Scale bar is 1 mm.

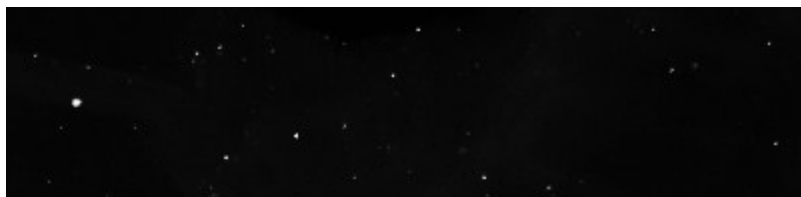
39

40 3. Additional Synchrotron XRF High-Z Maps

41 These maps represent elements detected in the full EDS spectra, but whose distributions could not

42 be visually correlated with biological structures.

43



44



45



46

47 Figure S4: From top to bottom, elemental maps of Cu, Fe and Ni in *M. musculus* distal radius and

48 ulna and carpal bones. Scan area is the same as in figure 1.

49

50 **4. Additional Standards for Synchrotron-Based XRF**

51 The Durango apatite standard used to calibrate and quality check the quantification data fits for
52 the *M. musculus* specimen has been analysed using a multitude of techniques including
53 synchrotron XRF, microprobe (which uses Durango apatite as a standard) and ESEM. Below we
54 compare the concentrations of elements in Durango apatite presented in this study against other
55 geological standards JA-3 and JG-1A also analysed at the Diamond Light Source synchrotron
56 (DLS), beamline I-18. Results show that Durango apatite is well constrained and a reliable
57 standard to use in synchrotron XRF analyses (table S1) and that the concentrations presented in
58 the study are reliable.

59

Durango Apatite Standardization

	<u>2016 session SR-XRF</u>	<u>2015 session SR-XRF</u>	<u>2014 session SR-XRF</u>	<u>EPMA</u>	<u>Bead XRF</u>	<u>PIXE XRF</u>	<u>Durango Apatite^{xx}</u>	<u>Durango Apatite^{yy}</u>
<u>P</u>	<u>18.20 %</u>	<u>n.a.</u>	<u>18.74 %</u>	<u>18.20 %</u>	<u>17.50 %</u>	<u>n.a.</u>	<u>17.8 %</u>	<u>18.1</u>
<u>Ca</u>	<u>38.20 %</u>	<u>38.19 %</u>	<u>38.80 %</u>	<u>38.20 %</u>	<u>38.80 %</u>	<u>46 %</u>	<u>38.61 %</u>	<u>38.72</u>
<u>Fe</u>	<u>540</u>	<u>397</u>	<u>621</u>	<u>280</u>	<u>203</u>	<u>333</u>	<u>420</u>	<u>430-510</u>
<u>Zn</u>	<u>40</u>	<u>27</u>	<u>49</u>	<u>b.l.d.</u>	<u>80</u>	<u>35</u>		<u>47</u>
<u>Sr</u>	<u>1400</u>	<u>669</u>			<u>516</u>	<u>982</u>	<u>510</u>	<u>70-915</u>
<u>La</u>			<u>5078</u>	<u>4154</u>				<u>2895- 4210</u>
<u>Ce</u>			<u>7802</u>	<u>5869</u>			<u>4440</u>	<u>270- 5640</u>
<u>As</u>			<u>1186</u>		<u>1100*</u>			<u>95-1050</u>

*Laser ablation ICP-MS

^{xx} Jarosewich et al.¹

^{yy} Marks et al.²

Glass Bead XRF Standardization
(all oxide wt. %)

	<u>JA3</u>		<u>JG1A</u>	
	<u>Bead XRF</u>	<u>Reference</u>	<u>Bead XRF</u>	<u>Reference</u>
<u>SiO₂</u>	<u>62.74</u>	<u>62.26</u>	<u>73.79</u>	<u>72.19</u>
<u>TiO₂</u>	<u>0.64</u>	<u>0.68</u>	<u>0.18</u>	<u>0.25</u>
<u>Al₂O₃</u>	<u>15.55</u>	<u>15.57</u>	<u>13.77</u>	<u>14.22</u>
<u>Fe₂O₃</u>	<u>6.50</u>	<u>6.59</u>	<u>1.95</u>	<u>2.05</u>
<u>MnO</u>	<u>0.11</u>	<u>0.11</u>	<u>0.07</u>	<u>0.06</u>
<u>MgO</u>	<u>3.49</u>	<u>3.65</u>	<u>0.58</u>	<u>0.69</u>
<u>CaO</u>	<u>6.31</u>	<u>6.28</u>	<u>2.14</u>	<u>2.13</u>
<u>K₂O</u>	<u>1.40</u>	<u>1.41</u>	<u>4.08</u>	<u>4.01</u>
<u>Na₂O</u>	<u>3.16</u>	<u>3.17</u>	<u>3.36</u>	<u>3.41</u>
<u>P₂O₅</u>	<u>0.11</u>	<u>0.11</u>	<u>0.08</u>	<u>0.08</u>

60

61 **Table S1:** Synchrotron quantification of trace elements for the Durango apatite used in this study
 62 (top) given in ppm or weight percent (%). Techniques include Synchrotron- Radiation X-Ray
 63 Fluorescence (SR-XRF), Electron Probe Micro Analysis (EPMA), Bead XRF, Proton Induced X-
 64 ray Emission (PIXE) and Inductively Coupled Plasma Mass Spectrometry (ICP-MS). Quality
 65 checks were accomplished using the glass bead method by analysing two geological standards,
 66 JA-3 and JG-1A (bottom), in addition to the Durango apatite. Error for synchrotron quantification
 67 is ~10% of the absolute value.

68

69

70 **5. Quantification for *M. musculus***

71 ***Synchrotron***

72 To quantify element concentrations, multiple point analyses were undertaken by locating an area
73 of interest within the scan, driving the stage to the area, and collecting a full energy spectrum for
74 30 sec. Multiple point analyses are taken per area of interest to account for variation within the
75 sample. The setup at the Diamond Light Source allows for the exact motor positions to be saved
76 for each pixel, allowing for precise locations to be selected using the viewed elemental maps.

77 Point analyses are then processed through the PyMCA software³[H], which is used to fit point
78 spectra based on the raw EDS files and from the experimental parameters using a Durango apatite
79 standard of known elemental concentrations for calibration.

80

81 A 25 µm attenuation layer of keratin was added to account for the attenuation caused by soft
82 tissue still on the sample. This is based on the results found in the Environmental Scanning
83 Electron Microscope (ESEM) when looking at the attenuation of Ca and P. The influence of the
84 organic content within the bone and cartilage had to also be considered in order to calculate
85 elemental concentrations. Although elements associated with organics (H, O, C, N) are too light
86 to be detected by the set up at DLS, they do influence the stoichiometry of the sample matrix,
87 which is used by the PyMCA software in determining trace element concentrations.

88

89 ***ESEM***

90 Based on the attenuation of the Ca and P fluorescence from the bones, this layer must be 25
91 microns thick and has a stoichiometry similar to keratin. These variables were added as a filter
92 layer when analysing the synchrotron XRF data in PyMCA.

Element	Durango Standard	<i>M. musculus</i> soft tissue
C		53.9%
N		13.59%
O		28.36%
Si		1%
P	16.69%	1.34%
S		0.55%
Cl		0.58%
K		0.64%

93 Table S1S2: ESEM XRF quantification of trace elements in one-day postnatal *M. musculus*
94 forelimb soft tissue given in weight percent (%). Calibration was accomplished using a Durango
95 apatite standard.

96

97 **References**

- 98 1. V.A. Solé, E. Papillon, M. Cotte, P.H. Walter, and J. Susini, *Spectrochim. Acta B*, 2007,
99 62, 63-68. [E. Jarosewich, J.A. Nelen and J.A. Norberg, *Geostandards Newsletter*, 1980, 4,](#)
100 [43–47. doi: 10.1111/j.1751-908X.1980.tb00273.x](#)
- 101 2. [M.A.W. Marks, T. Wenzel, M.J. Whitehouse, M. Loose, T. Zack, M. Barth, L. Worgard,](#)
102 [V. Krasz, G.N. Eby, H. Stosnach, G. Markl., *Chem. Geol.*, 2012, 291, 241–255.](#)
- 103 3. V.A. Solé, E. Papillon, M. Cotte, P.H. Walter, and J. Susini, *Spectrochim. Acta B*, 2007,
104 62, 63-68.
- 105